International Journal of Minerals, Metallurgy and Materials
Volume 21, Number 12, December 2014, Page 1254
DOI: 10.1007/s12613-014-1035-1

Effects of sintering temperature on the microstructural evolution and wear behavior of WCp reinforced Ni-based coatings

Chuan-hui Chen[1,2], *Yang Bai*[1,2], *and Xu-chu Ye*[1,2]

1) College of Materials Science and Engineering, Nanjing University of Technology, Nanjing 210009, China
2) State Key Laboratory of Materials-oriented Chemical Engineering, Nanjing 210009, China
(Received: 22 February 2014; revised: 15 May 2014; accepted: 20 May 2014)

Abstract: This article focuses on the microstructural evolution and wear behavior of 50wt%WC reinforced Ni-based composites prepared onto 304 stainless steel substrates by vacuum sintering at different sintering temperatures. The microstructure and chemical composition of the coatings were investigated by X-ray diffraction (XRD), differential thermal analysis (DTA), scanning and transmission electron microscopy (SEM and TEM) equipped with energy-dispersive X-ray spectroscopy (EDS). The wear resistance of the coatings was tested by thrust washer testing. The mechanisms of the decomposition, dissolution, and precipitation of primary carbides, and their influences on the wear resistance have been discussed. The results indicate that the coating sintered at 1175ºC is composed of fine WC particles, coarse M_6C (M=Ni, Fe, Co, etc.) carbides, and discrete borides dispersed in solid solution. Upon increasing the sintering temperature to 1225ºC, the microstructure reveals few incompletely dissolved WC particles trapped in larger M_6C, Cr-rich lamellar $M_{23}C_6$, and M_3C_2 in the austenite matrix. $M_{23}C_6$ and M_3C_2 precipitates are formed in both the γ/M_6C grain boundary and the matrix. These large-sized and lamellar brittle phases tend to weaken the wear resistance of the composite coatings. The wear behavior is controlled simultaneously by both abrasive wear and adhesive wear. Among them, abrasive wear plays a major role in the wear process of the coating sintered at 1175ºC, while the effect of adhesive wear is predominant in the coating sintered at 1225ºC.

Keywords: particle reinforced composites; composite coatings; tungsten carbide; microstructural evolution; wear behavior; sintering temperature

1. Introduction

High-temperature corrosion resistant Ni-based/WC composite coatings have been widely used in chemical processing industries, with particular needs in heat exchanger tubes, fan blades, and so on [1–2]. The coatings essentially acquire extra high strength, high hardness, low coefficient of thermal expansion, wear resistance, and oxidization resistance from solid solution and primary reinforced carbides, such as WC and M_6C, which is expected to prevent excessive oxidation and strengthen grain boundary [3]. Moreover, the *in situ* formation of $M_{23}C_6$, M_7C_3, and M_3C_2 around the primary carbides during the solidification process greatly affects the mechanical properties on the basis of their morphology, particle size, and distribution. The transformations of different carbides greatly depend on the service temperature of these workpieces.

In general, WC reinforced metal matrix composite coatings can be prepared by various surface techniques, including thermal spraying, arc welding, and laser cladding. However, there are still some uncontrolled factors such as phase composition, porosity, oxidization, and cracks [4–6]. Besides, these fast solidification techniques bring about dramatic decarbonization and low deposition rate, due to the uncontrolled ultra high temperature, high gas velocity, and residual oxygen.

Hexagonal tungsten carbide is a very stable material with ultra high hardness at room temperature. However, its good wettability and a certain amount of solubility in molten metals may cause series transformations in M/WC systems at ultra high temperature. These transformations are often controlled by the diffusion rate of the metal atoms at the

Corresponding author: Xu-chu Ye E-mail: yexuchu@njtech.edu.cn

solid/liquid boundary and metal melts at high temperature [7]. The evolution of primary MC (metallic carbides) decomposition in Fe-based alloys has been investigated for decades. The classic decompositions, namely, MC + γ → M_6C + γ′ and MC + γ → $M_{23}C_6$ + γ′ have been reported in various systems [8].

It is well known that M_6C carbides are the most common brittle phase present in M–W–C (M = Fe, Ni, Co, Cr, and so on) superalloy systems, which can effectively block the movement of dislocations. Furthermore, in certain systems, M_6C decomposes into $M_{23}C_6$ [9–10]. The Cr-rich $M_{23}C_6$ is also a stable phase that may result from the reaction WC + xCr → W + Cr_xC. The metallic tungsten formed as a result of WC decomposition tends to solubilize into the matrix until it approaches the solubility limit [11]. Thus far, different morphologies of $M_{23}C_6$, including the coarse lamellar line near grain boundaries, discrete particles, and nano-scaled particles, have been investigated in superalloys.

However, to the best of our knowledge, systematic studies on the effect of sintering temperature on the composition, microstructure, and wear resistance of vacuum sintered Ni-based/WC composite coatings, especially the microstructure evolutions at different temperatures, have been rarely reported in the literature. To this end, in this study, we have made an attempt to obtain a comprehensive understanding of the evolution of carbides in a Ni-based/WC metal-ceramic system. For this, the composite coatings were sintered at different temperatures at around the transformation points (1020 and 1223°C). The sintering temperature was controlled so as to avoid the over sintering or insufficient sintering of the coatings. Microstructural evolutions, including MC decomposition, subsequent M_6C decomposition, and $M_{23}C_6$ and M_3C_2 precipitation behaviors, have been investigated systematically.

2. Experimental

In this study, Co-coated WC (12wt% Co) and Ni-based alloy powders were used as raw materials. The chemical composition of the raw materials is listed in Table 1. Transformation stages in the Ni-based/WC (50wt% WC) composite system were analyzed by thermal analysis at a heating rate of 10°C/min in argon atmosphere, similar to the vacuum sintering conditions.

Table 1. Chemical composition of the raw materials wt%

Raw materials	Ni	Fe	Cr	Co	B	Si	C	W
Ni-based alloy	Bal.	10	8.5	—	3.0	3.5	0.7	—
WC	—	—	—	12	—	—	5.29	82.71

In the typical process, the precursor powders were mixed at a weight ratio of 1:1, and then pressed onto an AISI 304 stainless steel substrate under 200 kN. Polyvinyl alcohol (PVA) solution was used as the binder for the powder. Upon complete drying, the semi-finished samples were sintered in vacuum (<5 Pa) at a heating rate of 10°C/min from room temperature to the pre-set temperature. The samples were held at the desired temperature for 0.5 h and then cooled down to room temperature in the furnace, with an initial cooling rate of about 50ºC/min. During the sintering process, the coatings were held at 400°C additionally for a time period of 0.5 h, in order to exhaust the gases decomposed from the organic binder. The sintered composite coating thus obtained is 1.5–2.0 mm in thickness. For subsequent analysis of the samples by X-ray diffraction (XRD), scanning electron microscopy (SEM), and transmission electron microscopy (TEM), the coated samples were cut into small pieces and polished. Samples for TEM analysis were polished to a thickness of 50 μm, punched into ϕ3 mm, and finally thinned by iron beam until a hole is formed. A demagnetizer was used to weaken the magnetic effect of the samples on the focusing system.

The wear samples were cut into pieces of dimension 15 mm × 10 mm × 3 mm, followed by polishing using silicon carbide abrasive paper, and ultrasonic cleaning in acetone. The microhardness of the samples was measured by Vicker microhardness tester with a load of 1.96 N and a holding time of 15 s. The wear test was performed in compliance with the standards of ASTM G133-05, procedure A — unlubricated wear testing at room temperature. The test conditions adopted are the normal force of 40.0 N, the stroke length of 10.0 mm, the oscillating frequency of 5.0 Hz, the test duration of 2000 s, and the ambient temperature of 23–25°C.

3. Results and discussions

3.1. Thermal behavior

The differential thermogram obtained during the heating of Ni-based/WC (50wt%WC) powders is shown in Fig. 1. The thermogram shows three main peaks that signify the transformation temperature of the composite powders. Besides, three endothermic peaks of transformation points can be characterized. According to the sintering results, the pre-coating materials melt and form coatings at temperature over 1020ºC, which corresponds to the melting point of the Ni-based alloy. In general, tungsten carbide is chemically stable. Hence the WC powders do not transform or react at relatively low temperatures. However, the carbide can dis-

solve into metallic solutions at the interface between the liquid Ni-based matrix and tungsten carbide. This diffusion may cause several results: (1) reduction in WC volume fraction among coatings, which may also weaken the strengthening effect of the reinforcing particles; (2) dissolution and precipitation mechanisms lead to new precipitations and composites, which may enhance the matrix by solid solution strengthening and dispersion strengthening; (3) interfaces between carbide particles and the metal matrix form smooth transformation regions and attribute a higher bonding strength.

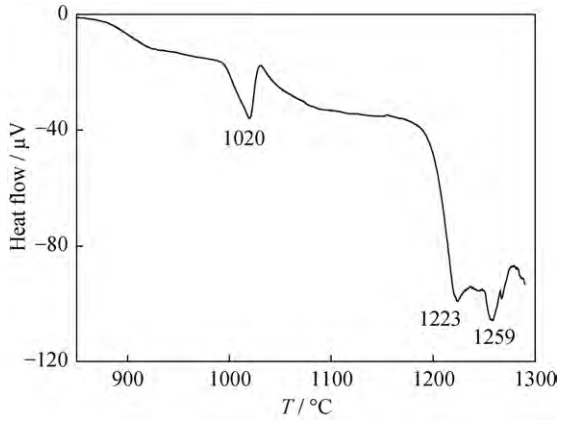

Fig. 1. DTA curve of Ni-based/WC (50wt% WC) powders.

The peak at around 1223°C refers to the phase transformation point of $M_6C \rightarrow M_{23}C_6 + M$ (M = Fe, Cr, Co, W) [12]. According to the calculated results of WC decomposition reactions on the basis of Kirchhoff's law, the temperature 1259°C corresponds to the decomposition point of $2WC = W_2C + C$ at 1250°C [13]. A higher sintering temperature is unfavorable for the coatings, since the bonding matrix might melt and flow away without facilitating the formation of wear resistant coatings.

3.2. XRD analysis

The structures and phases of the coatings sintered at different temperatures were analyzed by XRD using Cu K_α radiation. Fig. 2 shows the XRD patterns of Ni-based/WC (50wt% WC) composite coatings sintered at 1175 and 1225ºC for 0.5 h, recorded at the middle of the vertical cross-section. These XRD patterns indicate that the main phases in the coatings are the austenite matrix and complex carbides, such as M_6C and $M_{23}C_6$. Considering the disappearance of WC phase, it is believed that the decomposition of WC occurred at high temperature over the transformation point of 1223ºC. Besides, the XRD patterns of the sintered coatings did not show the presence of W_2C or WC_{1-x} at these two temperatures. Compared with the XRD pattern of the precursor powders, a large amount of M_6C (M = Ni, Cr, Fe) phase was formed over the melting temperature of the Ni-based alloy; while the peaks corresponding to $M_{23}C_6$ carbides appeared instead of WC peaks.

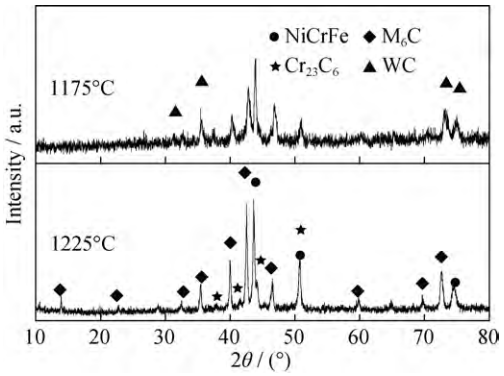

Fig. 2. XRD patterns of Ni-based/WC (50wt% WC) coatings sintered at different temperatures.

Thus, the reversible reaction between M_6C and $M_{23}C_6$ mostly depends on sintering temperature rather than sintering time. It has been reported that M_6C exists in a wide variety of C–W–M systems (M = Fe, Co, Ni) [11,14]. For sintering temperatures ranging from 650 to1000°C, M_6C carbides are metastable and may partly degenerate into $M_{23}C_6$ and M (M = W, Ni, Cr, Mo).

3.3. Microstructure

Fig. 3 shows the cross-sectional morphologies of the coatings sintered at 1775 and 1225ºC. The overall distribution of carbides in these two coatings can be observed in Figs. 3(a) and 3(b). In the case of the coating sintered at 1175ºC, most WC particles in the upper region, closer to the coating surface, maintain their original shape and size even after sintering for 0.5 h (Fig. 3(c)). It can be seen that a large quantity of fine carbide particles (<10 μm) precipitate in the austenite matrix. However, bar-like secondary carbides begin to form in large scale from the bottom region of the coating (Fig. 3(a)). This could possibly correspond to M_6C, as determined from the XRD results. On contrary to the phase composition of the coating sintered at 1175ºC, the coating sintered at 1225ºC reveals more complicated composition of lamellar and blocky phases over 100 μm in the metal matrix (Fig. 3(b)). The brighter phase, which uniformly fills the coating, is much larger than the original size of the WC particles.

For most Ni-based alloys, M_6C carbides are derived from the degradation of MC carbides as $MC + \gamma \rightarrow M_6C + \gamma'$. However, in the Ni-based/WC system considered in this study, the low melting alloy melts that surround the WC

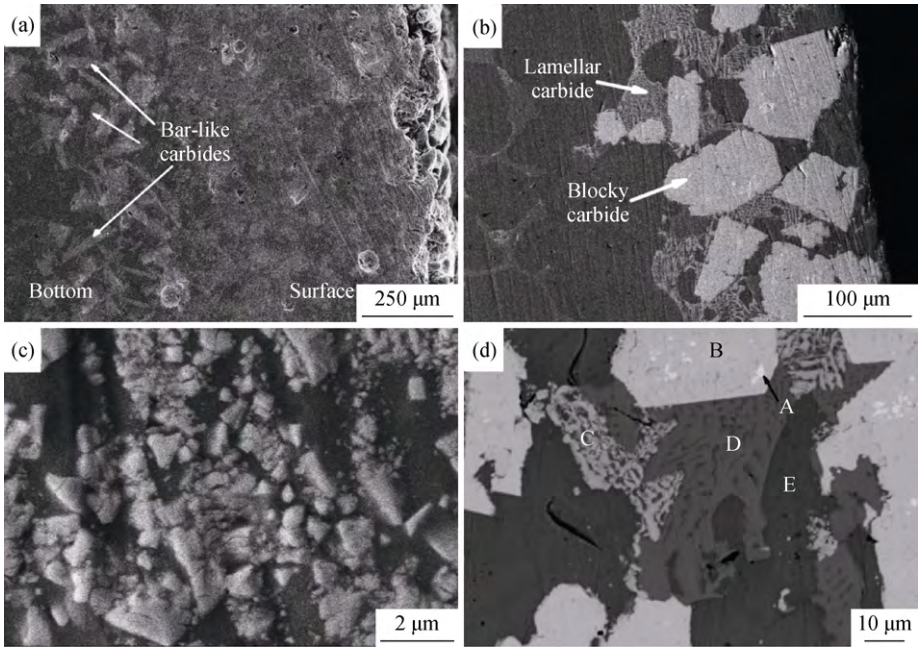

Fig. 3. Cross-sectional SEM images of the coatings sintered at 1175°C (a) and 1225°C (b); (c) and (d) high magnification images of (a) and (b), respectively.

particles and carbide dissolve into the liquid matrix from interfaces between the solid/liquid boundaries. The free elements W and C react with the other iron group elements (Ni, Cr, Fe, etc.) to form secondary carbides, which disperse in the matrix during the solidification process. Also, the decomposition of MC to M_6C is common in the iron group element–WC system, while the subsequent reaction $M_6C \rightarrow M_{23}C_6 + M$ is rather difficult [14]. The chemical composition of M_6C carbides is usually rich in W, Ni and Fe, and poor in Cr. On the other hand, $M_{23}C_6$ is usually rich in Cr. The $M_{23}C_6$ and M_6C carbides belong to $Fm\bar{3}m$ and $Fd\bar{3}m$ face centered cubic (fcc) space groups, respectively, and have similar miller indices and crystal structures. As is well known, $M_{23}C_6$ carbides form alloys in two different ways [15]. One is via the decomposition of M_6C and MC, and the other is via the direct precipitation of carbides from the metal matrix. As can be seen from the SEM image shown in Fig. 3(d), other forms of carbides surround M_6C carbides as cellular dendrites. The backscattered electrons, which yield a higher phase contrast when compared to the secondary electrons, indicate five different phases of carbides, since the mean atomic number of these carbides are different. Large blocky carbides form based on the fine WC particles. However, there are still a small amount of undissolved WC particles trapped in large M_6C carbides (A in Fig. 3(d)). The decomposition of MC into M_6C is accelerated and yet another formation of $M_{23}C_6$ takes place in the matrix at the higher temperature.

Table 2 lists the chemical composition of different precipitates in the coating sintered at 1225ºC for 0.5 h (marked in Fig. 3(d)). As is seen, the precipitates A, B, and E are WC, M_6C, and the γ matrix, respectively. The precipitate C is rich in W, and deficit of Fe and Cr. On the other hand, the precipitate D is rich in Fe and Cr, and poor in W. Further TEM observation indicates that these two precipitates are M_3C_2 and $M_{23}C_6$, respectively, which are both conjoint with blocky M_6C. Moreover, these carbides can form quite far from M_6C carbides, which cannot be explained by the decomposition and diffusion of M_6C. This phenomenon may be attributed to the segregation of Cr. Given the facts that these two carbides are usually rich in Cr and more stable than M_6C [16].

Table 2. Chemical composition of different phases in the composite coating sintered at 1225°C for 0.5 h (in Fig. 3) wt%

Position in Fig. 3	C	Si	Cr	Ni	Co	Fe	W
A	23.49	4.75	3.38	2.07	1.58	9.75	54.98
B	25.48	—	5.64	6.87	—	8.14	53.87
C	23.24	—	14.88	17.04	—	5.28	39.59
D	23.45	—	29.10	26.79	—	3.34	17.30
E	27.87	3.36	9.28	40.45	—	18.34	—

The TEM analysis of the coating sintered at 1175ºC (Fig. 4 (a)) reveals dark WC carbide precipitates in bright γ phase. The corresponding selected area electron diffraction pattern indicates rectangular and triangular-shaped dark precipitates,

which respectively refer to block-like and prism-like particles with the same phase as that of WC in the same orientation of [011]. The particle size of WC is less than 10 μm. Besides, M_6C carbides are formed at the bottom region of the coating. No other carbides, like $M_{23}C_6$, can be found at the grain boundaries of WC or M_6C/γ that precipitate directly from the matrix via segregation. So it can be induced that the decomposition of MC occurs at this low temperature, but no further degradation reaction takes place in this system. On the basis of results reported in previous studies, the decomposition of MC at this temperature can be described as $MC + \gamma \rightarrow M_6C + \gamma'$.

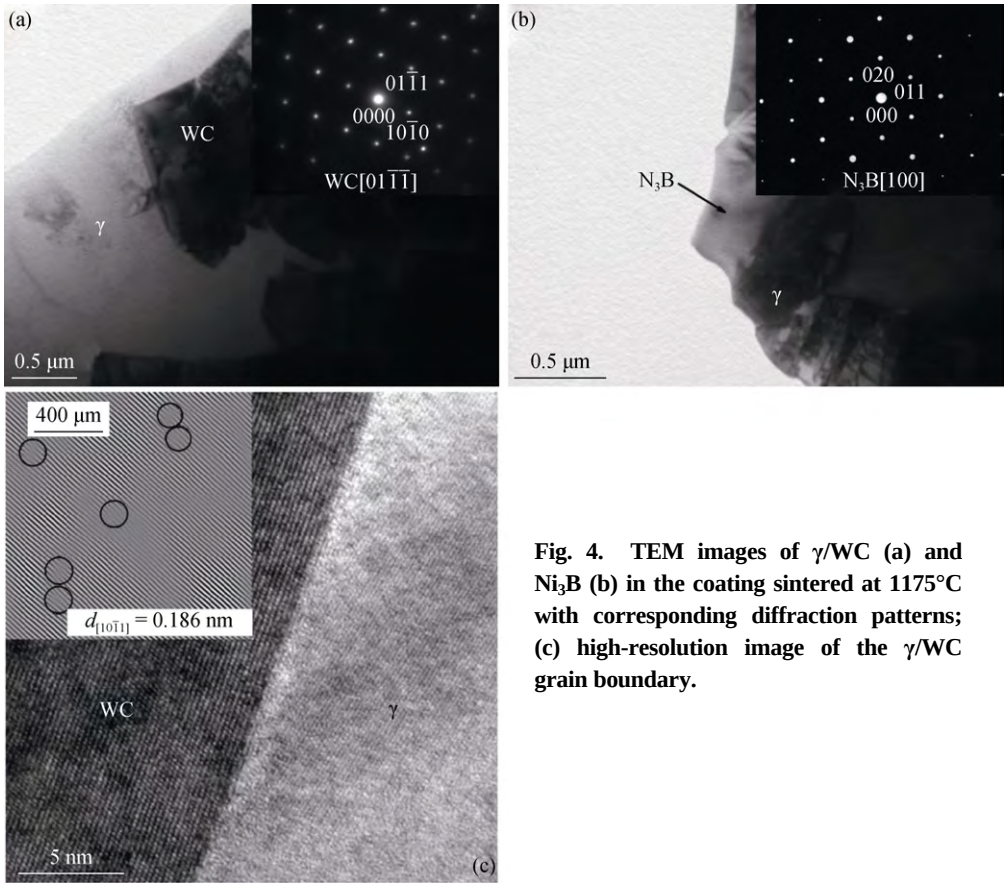

Fig. 4. TEM images of γ/WC (a) and Ni_3B (b) in the coating sintered at 1175°C with corresponding diffraction patterns; (c) high-resolution image of the γ/WC grain boundary.

Furthermore, yet another rare precipitate has been found in the metal matrix. The bright field TEM image and the [100] SAED pattern confirm that the precipitate is Ni_3B of orthorhombic space type with lattice parameters of approximately a = 0.5025 nm, b = 0.664 nm, and c = 0.442 nm, as shown in Fig. 4 (b). In general, the Ni-based coatings have interdendritic lamellar eutectic of γ-Ni_3B. This boride nucleates along the grain boundaries ofγ phase, and grows in the lamellar form during eutectic solidification. However, with decrease in the concentration of boron in the Ni-based/WC system, the higher carbon concentration promotes the formations of carbides and seizes the metal element from the matrix. As a result, boride can hardly be observed in the composite coatings with high carbon content.

In general, the mechanical properties of these coatings usually depend on the microstructure of different phases and their grain boundaries. The high resolution TEM image of the coating sintered at 1175ºC (Fig. 4 (c)) reveals a very low dislocation density of the Ni matrix and a higher dislocation density of WC. There are 7 defects per 133 nm^2 in (10$\bar{1}$1). The dihedral angle of the interface between WC (10$\bar{1}$0) and austenitic matrix (111) is measured to be 11.53°. Therefore, the presence of defects or grain boundaries, which act as heterogeneous nucleation sites, may greatly promote the decomposition and grain growth rate.

With increase in sintering temperature to 1225ºC, several new carbides precipitate in the matrix, as shown in Fig. 5. The SAED analysis and the corresponding high resolution TEM images are illustrated in Fig. 6. Besides the austenite matrix (marked as A), the remaining precipitates marked as B, C, and D are M_3C_2, M_6C, and $M_{23}C_6$, respectively. Lamellar Cr_3C_2 is formed at two places, namely, at the grain

boundary of austenite/M_6C, and at the matrix nearly parallel to the grain boundary of austenite/M_6C, with a gap of about 1 μm. Accordingly, the morphology of lamellar M_3C_2 proves that the carbides can be formed both by the degradation of M_6C and by the segregation of Cr and Fe directly in the austenite matrix. The former reaction can be expressed as $M_6C + \gamma \rightarrow M_3C_2+\gamma'$. According to the SEM image, $M_{23}C_6$ can also be formed at the interfaces of M_6C/austenite and M_3C_2/austenite. The corresponding EDS analysis of $M_{23}C_6$ shown in Tables 2 and 3 indicate that, although they are both rich in Cr and Fe, $M_{23}C_6$ close to M_6C has a higher Cr/Fe ratio and lesser W content when compared to that far from M_6C. It has been reported that the Cr concentration in the matrix increases with increase in temperature [4], while the diffusion rate of C is much faster than that of Cr in alloys. As a result, the formation of carbides is controlled by the diffusion of the metal element. The possibility of Cr to form $M_{23}C_6$ is feasibly via the degradation of M_3C_2 and M_6C. With increase in distance to the prime carbides, more Cr atoms dissolve into the matrix, consistent with that reported in previous studies [8].

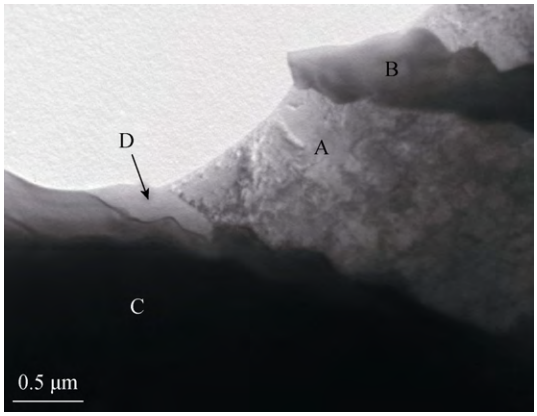

Fig. 5. TEM image of the coating sintered at 1225°C (A — austenite, B — M_3C_2, C — M_6C, and D — $M_{23}C_6$).

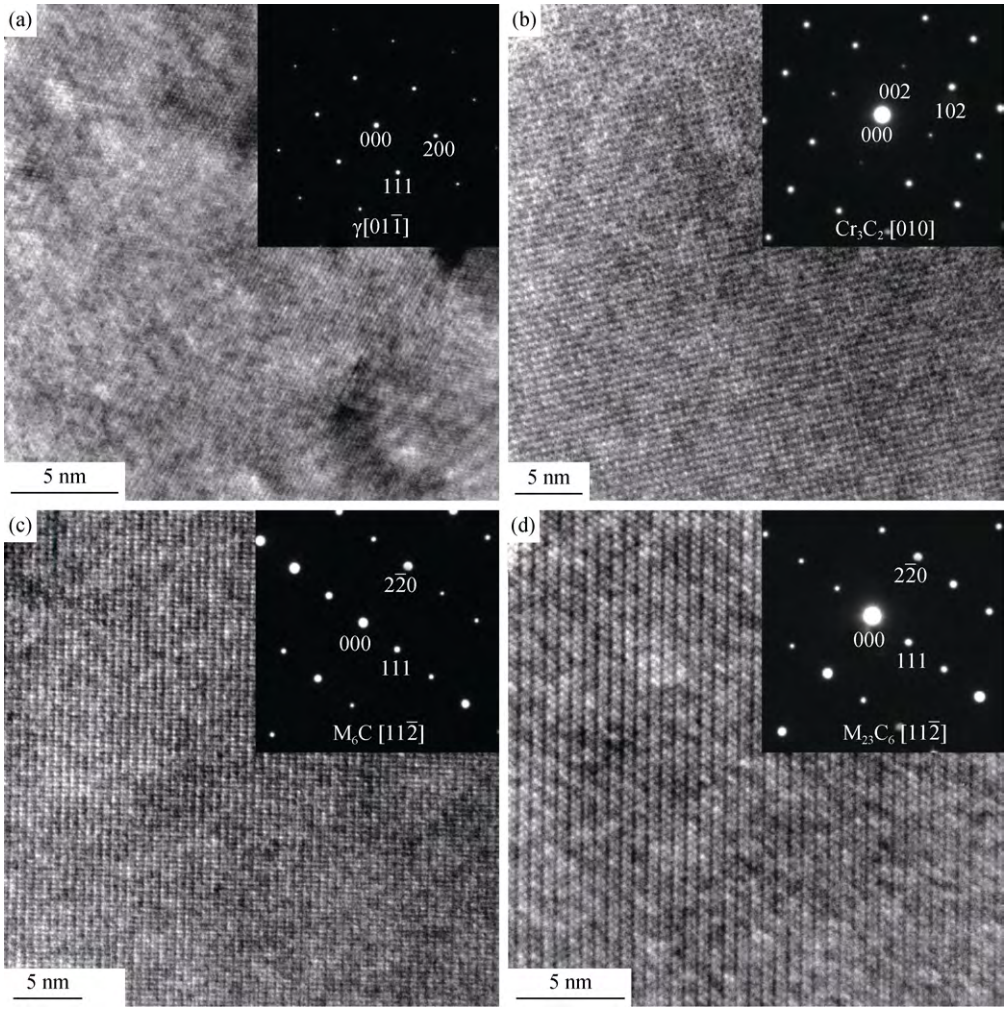

Fig. 6. High-resolution TEM images revealing different phases in the coatings sintered at 1225°C: (a) austenite; (b) M_3C_2; (c) M_6C; (d) $M_{23}C_6$.

Table 3. Chemical composition of different phases in the composite coating sintered at 1175°C for 0.5 h (in Fig. 5) wt%

Position in Fig. 5	Fe	Ni	Cr	W
A	51.41	25.76	12.52	10.32
B	9.93	1.98	15.19	72.9
C	11.77	5.04	6.42	76.78
D	27.59	4.02	38.61	29.78

3.4. Mechanical properties

In general, the wear resistances of the coatings depend on various factors: phase composition, grain size or particle size of the enhanced phases, distribution of the enhanced phases, matrix/precipitate bonding strength, and so on. The Vickers hardness number of the coating sintered at 1175°C ranges from 399 to 562 HV. The presence of fine carbide particles increases the average hardness of the alloys, thereby preventing abrasive wear and adhesive wear. The Vickers hardness number of the coating sintered at 1225°C ranges from 349 to 420 HV for the matrix and 1023 to 1345 HV for large precipitates.

The Vickers hardness of hexagonal WC, $Cr_{23}C_6$, M_6C (Fe_3W_3C) and Cr_3C_2 are 2400, 976, 2210 and 2280 HV, respectively. Here the chemical composition of M (M = Ni, Cr, Fe, Co, W) plays an important role in determining the real hardness of these carbides. In general, erosive wear caused by plastic deformation in a pure metal system is mainly influenced by its hardness [17–18]. On the other hand, with the addition of a large quantity of hard particles, the fracture toughness is greatly influenced by the composition of the material.

The fracture toughness reduces with increase in the particle size of the reinforced phases. Uniform distribution of fine particles reduces the opportunity of crack formation during the wear process. The wear losses in the coatings sintered at 1175°C and 1225°C are respectively 0.8 and 4.1 mg during 2000 s. Although the coating sintered at 1175°C shows a higher wear resistance, its friction coefficient is slightly higher than that of the coating sintered at 1225°C, as shown in Fig. 7. The stage during the first 400 s presents a rising trend for both the coatings as a period of surface destruction. As a result of surface cracking, the abrasive wear causes an increase in friction coefficient. After 400 s, the friction coefficients of both the coatings tend to be stable till the end of the tests. The decreasing peaks in the coating sintered at 1225°C may refer to the cracking of larger carbides. Accordingly, it can be concluded that the fine WC dispersed uniformly in the Ni-based matrix is optimum for wear resistance. Tungsten carbide reinforced coatings have high wear resistance due to the presence of WC particles. These coatings consist of the Ni-based matrix that serves as a binder for fine and uniformly distributed WC particles. This unique morphology leads to higher hardness and fracture toughness compared with the coatings that consist of a diluted matrix fulfilled with decomposed and grown carbides. The WC particles protect the matrix from direct contact with the wear medium, although the metallic binder has low wear resistance.

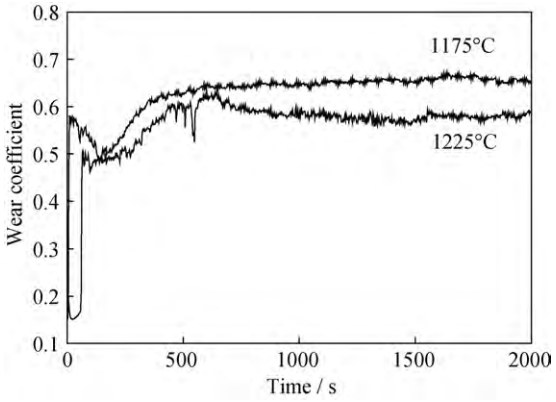

Fig. 7. Wear coefficients of the coatings sintered at 1175°C and 1225°C.

The typically morphology of wear track on the surface of the coatings sintered at 1175 and 1225°C are shown in Fig. 8. Grooves caused by abrasive wear and pits caused by spalling hard particles can be observed in both coatings. The

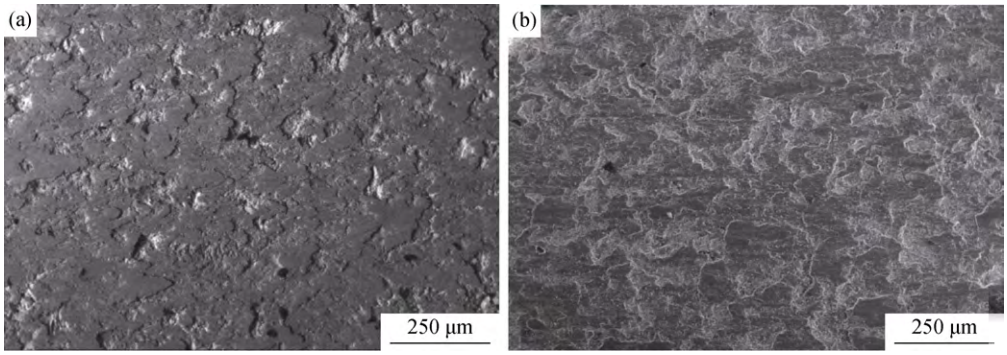

Fig. 8. SEM images of wear track on the surface of the coatings sintered at 1175°C (a) and 1225°C (b).

morphology of the coating sintered at 1225°C shows large-sized flaky exfoliation of the material and longer grooves compared with the coating sintered at 1175°C. This phenomenon may contribute to the formation of larger-sized carbides at a higher sintering temperature. Densely distributed undissolved WC particles can inhibit the formation and propagation of the cracks, along with the groove formation that usually occurs in the soft matrix.

The wear behavior during continuous grinding was further analyzed by observing wear debris. Wear debris from both the coatings present different sizes and chemical compositions, as shown in Figs. 9(a)–9(d) and the corresponding EDS results (Figs. 9(e) and 9(f)), respectively. The size of most wear debris from the coating sintered at 1175°C is less than 20 μm. EDS results of all the particles shown in Fig. 9(c) indicate that the debris is rich in Ni and W. Fig. 9(b) illustrates the debris over the size 150 μm spalled from the coating sintered at 1225°C, with some cracks on the surface. This debris is rich in Fe and Cr, and low in Ni and W, compared with that from the coating sintered at 1175°C. Accordingly, it can be concluded that the large debris contains more austenite. C atoms decomposed from the fine carbides precipitate onto larger carbides as M_6C to promote the growth of the larger precipitates. Cracks occur along the grain boundaries between metal and carbides and the corresponding debris tend to be large pieces of the metallic matrix and carbides. The coating sintered at 1175°C presents the characteristics of abrasive wear, including the tough surface and holes formed by spalling. Nevertheless, obvious grooves caused by the hard particles and exfoliations prove that adhesive wear plays an important role in the friction process.

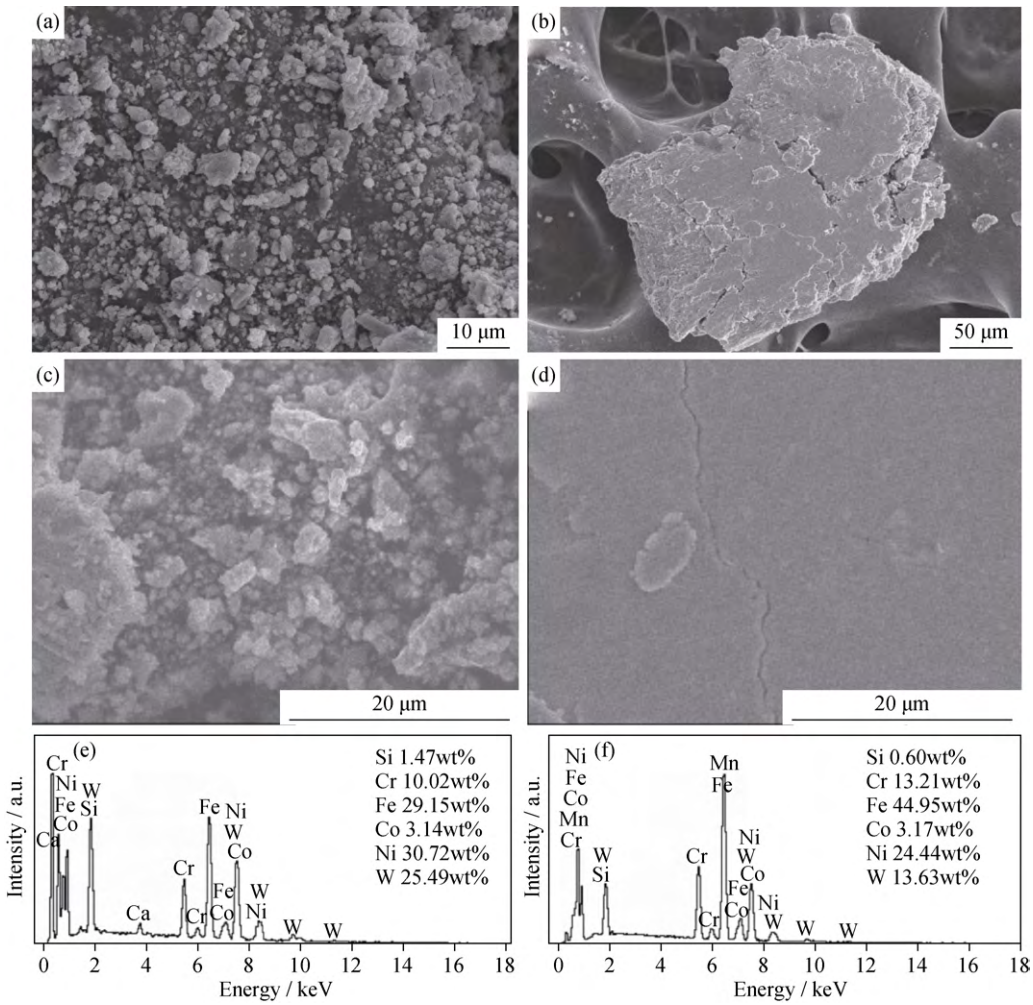

Fig. 9. Morphologies of wear debris from the coatings sintered at 1175°C (a), 1225°C (b), and the corresponding EDS analysis results ((c) and (e) for (a); (d) and (f) for (b)).

4. Conclusions

(1) M_6C is formed by the decomposition of WC in the liquid Ni-based matrix according to the dissolution and precipitation mechanisms. New carbides, namely, $M_{23}C_6$ and M_3C_2, are formed in the coating sintered at 1225°C, with the

transformation point (1223°C) corresponding to the reaction $M_6C \rightarrow M_{23}C_6 + M$.

(2) The formation of M_6C begins with the appearance of the liquid phase. High temperature sintering promotes the growth of blocky M_6C precipitates. Sintering at a higher temperature (1225°C) above the transformation point results in the formation of lamellar Cr-rich $M_{23}C_6$ and M_3C_2 carbides in two positions, namely, the γ/M_6C grain boundary and matrix closer to M_6C. No discrete carbides have been found in the coating sintered at 1225°C, due to a faster diffusion of C at a higher temperature.

(3) The coating sintered at 1175°C has a higher wear resistance due to the uniform distribution of fine WC particles. Although the coating sintered at 1225°C contains high hardness carbides, it has low wear resistance owing to the larger size and low fracture toughness.

Acknowledgements

The authors gratefully acknowledge the financial support of the Program for Changjiang Scholars and Innovative Research Team (PCSIRT) in Chinese Universities (No. IRT1146).

References

[1] D.S. Xiong, Lubrication behavior of Ni–Cr-based alloys containing MoS_2 at high temperature, *Wear*, 251(2001), No. 1, p. 1094.

[2] S.H. Si, X.M. Yuan, Y.L. Liu, Y.Z. He, and S. Keesam, Effect of laser power on microstructure and wear resistance of WC_P/Ni cermet coating, *J. Iron Steel Res. Int.*, 13(2006), No. 3, p. 74.

[3] Q. Li, T.C. Lei, and W.Z. Chen, Microstructural characterization of WCp reinforced Ni–Cr–B–Si–C composite coatings, *Surf. Coat. Technol.*, 114(1999), No. 2-3, p. 285.

[4] N. Espallargas, J. Berget, J.M. Guilemany, A.V. Benedetti, and P.H. Suegama, Cr_3C_2–NiCr and WC–Ni thermal spray coatings as alternatives to hard chromium for erosion-corrosion resistance, *Surf. Coat. Technol.*, 202(2008), No. 8, p. 1405.

[5] M. Aristizabal, N. Rodriguez, F. Ibarreta, R. Martinez, and J.M. Sanchez, Liquid phase sintering and oxidation resistance of WC–Ni–Co–Cr cemented carbides, *Int. J. Refract. Met. Hard Mater.*, 28(2010), No. 4, p. 516.

[6] C. Guo, J.M. Chen, J.S. Zhou, J.R. Zhao, L.Q. Wang, Y.J. Yu, and H.D. Zhou, Effects of WC–Ni content on microstructure and wear resistance of laser cladding Ni-based alloys coating, *Surf. Coat. Technol.*, 206(2012), No. 8-9, p. 2064.

[7] C.M. Fernandes, A.M.R. Senos, and M.T. Vieira, Control of eta carbide formation in tungsten carbide powders sputter-coated with (Fe/Ni/Cr), *Int. J. Refract. Met. Hard Mater.*, 25(2007), No. 4, p. 310.

[8] J. Wang, L.Z. Zhou, X.Z. Qin, L.Y. Sheng, J.S. Hou, and J.T. Guo, Primary MC decomposition and its effects on the rupture behaviors in hot-corrosion resistant Ni-based superalloy K444, *Mater. Sci. Eng. A*, 553(2012), p. 14.

[9] A. Antoni-Zdziobek, J.Y. Shen, and M. Durand-Charre, About one stable and three metastable eutectic microconstituents in the Fe–W–C system, *Int. J. Refract. Met. Hard Mater.*, 26(2008), No. 4, p. 372.

[10] C.M. Fang, M.A. van Huis, and H.W. Zandbergen, Stability and structures of the CFCC-TmC phases: a first- principles study, *Comput. Mater. Sci.*, 51(2012), No. 1, p. 146.

[11] C.M. Fernandes, V. Popovich, M. Matos, A.M.R. Senos, and M.T. Vieira, Carbide phases formed in WC–M (M=Fe/Ni/Cr) systems, *Ceram. Int.*, 35(2009), No. 1, p. 369.

[12] B. Djerdjare, S. Lebaili, and S. Lay, Microstructural study of (Co–Ni–Fe) based alloys, *Mater. Sci. Eng. A*, 475(2008), No. 1-2, p. 336.

[13] Z.L. Li, Y.H. Jiang, X.M. Ye, and R. Zhou, Dissolution of tungsten carbide particulates (WC) in the matrix of WC reinforced gray cast iron matrix composite, *Acta Mater. Compos. Sin.*, 24(2007), No. 2, p. 13.

[14] C.M. Fernandes and A.M.R. Senos, Cemented carbide phase diagrams: a review, *Int. J. Refract. Met. Hard Mater.*, 29(2011), No. 4, p. 405.

[15] G.H. Bai, J.S. Li, R. Hu, T.B. Zhang, H.C. Kou, and H.Z. Fu, Effect of thermal exposure on the stability of carbides in Ni–Cr–W based superalloy, *Mater. Sci. Eng. A*, 528(2011), No. 6, p. 2339.

[16] T.S. Jo, J.H. Lim, and Y.D. Kim, Dissociation of Cr-rich $M_{23}C_6$ carbide in Alloy 617 by severe plastic deformation, *J. Nucl. Mater.*, 406(2010), No. 3, p. 360.

[17] Y.C. Lin and Y.C. Chen, Reinforcements affect mechanical properties and wear behaviors of WC clad layer by gas tungsten arc welding, *Mater. Des.*, 45(2013), p. 6.

[18] J.N. Li, H.Q. Li, M. Wang, S.F. Wang, Q. Ji, M. Li, and J. Chi, Applications of WC-based composites rapid synthesized by consumable electrode *in-situ* metallurgy to cutting pick, *Int. J. Refract. Met. Hard Mater.*, 35(2012), p. 132.